Experimental Study of the Flow in the Metering Nip of a Metering-Size Press

O. Réglat and P. A. Tanguy
Dept. of Chemical Engineering, École Polytechnique, Montreal, Quebec, Canada, H3C 3A7

The metering operation in the transfer-roll coating process is crucial for achieving a good uniformity and suitable thickness of the coating film. Experimental results carried out on a laboratory coater are reported. This coater mimics industrial flow conditions: it has a transfer roll and a metering-rod diameter similar to those found on a pilot coater, it operates at commercial speed, and the cover of the transfer roll is deformable. The experimental apparatus is described first. Then, a video analysis of the rib pattern is presented. Some interesting features are shown, in particular the existence of an inertia regime at high speed. The nip flow hydrodynamics are investigated using measurements of the pressure profile. It is shown that the film stability is strongly linked to the flow at the exit of the nip. The analysis of the maximum pressure in the nip, for various fluid viscosities and operating parameters, is represented using a master curve.

Introduction

The metering-size press (MSP) process is receiving increasing attention for the surface treatment of paper, due to its particular flexibility in dealing with a wide range of coat weights and base papers. The MSP principle is shown in Figure 1. The equipment is composed of a transfer roll and a backing roll, both covered with an elastomer. The rolls rotate at the same speed in a contrarotating mode. The paper web is fed in the application nip between the two rolls and picks up the coat that has been applied on the transfer roll beforehand. The amount of coating color on the transfer roll is controlled by a metering chrome-plated rod corotating with the transfer roll, but at a much lower speed.

Metering-size presses belong to the general category of roll coating devices. At high speed, these coating systems are known to generate flow instabilities and nonuniformities. This affects the coater runnability, and it results in the occurrence of defects on the coated film. Certain defects, like ribs, are formed at the exit of the metering nip. Others are generated in the application nip, mainly due to film splitting and coating color/paper interactions (Salminen et al., 1996).

Coater runnability and film-coating rheology are strongly interrelated. In the paper industry, the runnability of coating formulations is usually tested on pilot coaters. They provide greater flexibility for rapid grade changes and are less expensive to operate than mill coaters. A still cheaper alternative is the use of laboratory coaters, which are widely used for the preliminary screening of blade coating formulations (Eklund et al., 1988). In the field of MSP coating, none of the commercial laboratory coaters are of real use in formulation development: they either operate at low rotational speed, or lack a transfer roll. Moreover, the design of their metering unit is somewhat different from that found on a MSP. Thus, the coating flow generated in these laboratory coaters does not mimic the actual process.

From a flow-analysis standpoint, the metering system of a MSP (Figure 2) can be divided into three parts: the feed

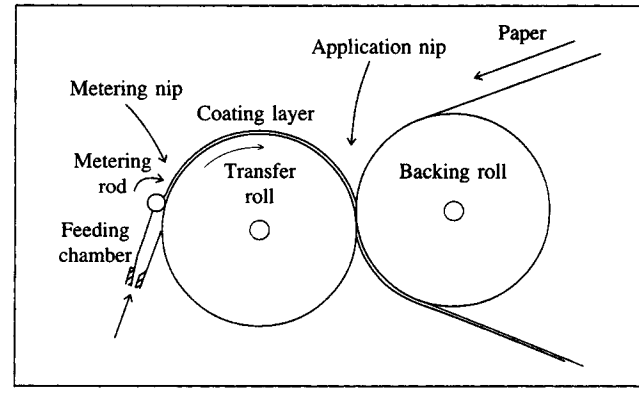

Figure 1. Metering-size press.

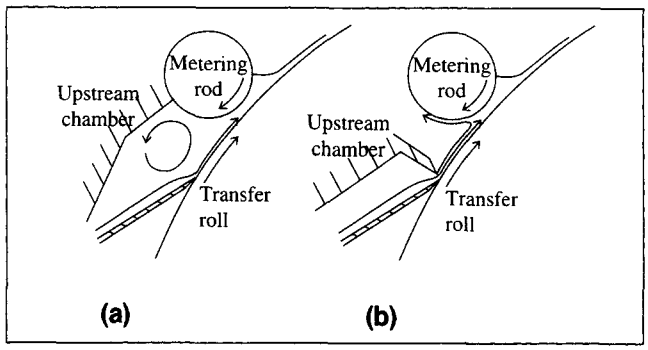

Figure 2. Metering nip: (a) confined design; (b) open geometry.

chamber, the nip gap, and the transfer roll. The color fed to the chamber is strongly accelerated when reaching the transfer roll upstream from the metering nip and can be subjected to flow instabilities. In the nip area, the fluid is submitted to very high shear rates (on the order of 10^6 s^{-1}) in a very short time (1 ms). Past the metering rod, it then relaxes almost immediately to a zero shear rate at the transfer-roll surface.

Two kinds of feed-chamber geometry can be used: the confined chamber and the open design (Figure 2). Industrial coaters running at high speed are generally equipped with a confined chamber. The hydrodynamics in such geometry is very similar to that of a short dwell pond. In short dwell coaters, highly unstable flows can be generated as evidenced by Aidun (1991a,b). Numerical simulations of the three-dimensional flow in the pond and the lubrication flow in the blade vicinity are very helpful in assessing the influence of these instabilities on the film uniformity (Miura and Aidun, 1992; Conlisk and Foster, 1991).

In more recent designs (Kustermann and Damrau, 1994), the chamber is replaced by a fountain applicator where the color is applied on the transfer roll as a thick layer. The fluid that does not go through the metering nip is then removed from the system. Such an open design yields completely different hydrodynamic flow patterns upstream from the metering rod, and may yield more stable flow than with the confined geometry.

In the metering nip, the gap between the two rolls is extremely small, of the order of 40 μm. Such a thin gap cannot be obtained with a pair of hard rolls, especially on the full width of mill coaters (up to 8 m). In practice, the transfer roll is covered with a soft elastomeric layer that eliminates the risk of clashing between the two rolls, and allows more tolerance on the runout (as a side benefit). The gap width cannot be imposed; rather, it results from an equilibrium between the elastic force due to the deformation of the elastomer, the pressure, possibly the normal stress induced in the nip contraction, and finally the overall load applied on the metering rod. Carvalho and Scriven (1993) performed numerical flow simulations, based on the lubrication theory, in the case of a soft nip. They used both one- and two-dimensional models to predict the roll deformation and compute pressure profiles in the nip. They distinguished positive and negative gaps, that is, both rolls are either initially compressed or not, while being at rest. They analyzed their results using an elastic number, earlier introduced by Coyle (1988), which represents the ratio of viscous forces in the nip vs. elastic forces in the cover, namely:

$$Ne = \frac{\mu V}{ER}, \tag{1}$$

where μ is the fluid viscosity, V is the average velocity of the two rolls, E is the Young's modulus of the deformable cover, and R is a characteristic roll radius based on the metering-rod radius, R_m, and the transfer-roll radius R_t, namely,

$$R = \frac{2}{\frac{1}{R_m} + \frac{1}{R_t}}. \tag{2}$$

Past the metering rod, the flow on the transfer roll is subject to ribbing. Ribs are always present on a metered transfer roll, although these nonuniformities, if they are small enough, may not affect the final product quality. A large amount of work has been devoted to these instabilities in roll coaters, but very few of them directly concern reverse-roll configuration and soft nips. Moreover, the design and operating conditions used in these studies differ significantly from the MSP process: roll radius ratio of 1 vs. 0.1 in a MSP, speed of 300 m/min against over 1,000 m/min in paper coating, and nip gap thicknesses well above 50 μm. These considerations make our application original, corresponding to an extreme case as compared to the available literature.

Stability to ribbing studies were initiated by Pearson in 1960. Based on the lubrication theory, he showed that the ribs result from an equilibrium between the surface tensions at the meniscus and the viscous forces through the nip. Pitts and Greiller (1961) developed a criterion on the onset of ribbing, showing that a negative pressure gradient at the exit of the nip always leads to a stable to ribbing pattern. Since then, other criteria have been proposed (Mill and South, 1967; Greener et al., 1980; Benkreira et al., 1982), based on a critical capillary number (viscous forces over surface tension forces), expressed as a function of a dimensionless gap thickness:

$$Ca = \frac{\mu V_t}{\sigma} = a\left(\frac{H_0}{R}\right)^{\alpha}. \tag{3}$$

The wide variety of values obtained of a (from 13.5 to 7,500) and α (from 1 to 2) are likely due to the difficulty the authors faced in telling stable from unstable patterns.

Coyle (1984) examined both ribbing and cascade phenomena in reverse-roll coaters. He explained that the cascade phenomenon was due to air entrapment from the exit of the nip, showing that it occurs only at a relatively high velocity ratio (the metering-rod velocity V_m vs. the transfer-roll velocity V_t must be at least greater than 0.2). Based on experimental measurements, he built some stability diagrams representing stable and unstable areas with respect to both ribbing and cascade phenomena, as a function of the velocity ratio V_m/V_t and the capillary number. Two-dimensional finite-element

simulations were used to interpret the role of these two parameters on the coating hydrodynamics: they tend to pull the meniscus through the gap, and then to reduce the recirculations under the meniscus. Stability diagrams built for different fluid viscosities revealed that inertia effects become nonnegligible for the only case experimented with a low viscosity fluid (80 mPa·s). Later, Coyle et al. (1990a) pursued their study, and found that an increase of either the gap thickness or the Reynolds number can widen the stable area in their stability diagram. Inertia effects, even if very low as compared to capillary ones, can increase the value of the critical capillary number, and then delay the onset of ribbing. However, there is apparently no effect of inertia at low velocity ratio. In another study on forward roll coating, the same authors (Coyle et al., 1990b) numerically investigated the effect of a perturbation in the transverse direction. According to this study, a two-dimensional stable flow tends to bifurcate to a three-dimensional unstable ribbed flow. They could accurately predict the critical capillary number at which this bifurcation occurs, and also showed some secondary effects: an increase in the Reynolds number stabilizes the short wavelengths (or rib widths) and destabilizes the long ones.

The objective of the present work is to address the general problem of flow instabilities in the MSP process. For this purpose, a laboratory coater has been designed and built. This coater, which mimics the metering unit of a MSP, is used to investigate the flow phenomena occurring during the formation of the film on the transfer roll. After a description of this laboratory coater, a first series of results with simple Newtonian fluids is presented. This series includes visualizations of the ribs on the film and measurements of the pressure profile in the metering nip.

Laboratory Coater

The experimental apparatus is presented in Figure 3, and the design parameters are given in Table 1. The transfer roll is covered with a SBR layer (Dynacote, StoweWoodward), with a thickness of 15 mm. The metering rod is chrome-plated. The load is applied on the metering rod by two air cylinders fixed at both ends. The velocities of the transfer roll and the metering rod, and the load applied on the metering rod can be adjusted independently. The present design is based on an upstream chamber with an open geometry. The thickness of the coating layer applied on the transfer roll before the metering nip varies from 1 mm to 10 mm. The excess of color is removed by the metering rod, which is itself scraped with a doctor blade.

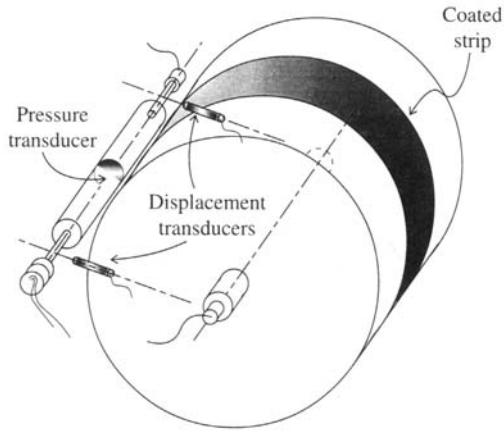

Figure 3. Laboratory coating rig.

Table 1. Laboratory Coater Parameters

Transfer roll	Diameter	800 mm
	Rotational velocity	0 to 1,100 m/min
	Runout	5 μm
	Hardness	60 P&G
Metering rod	Diameter	80 mm
	Rotational velocity	0 to 200 m/min
	Runout	5 μm
	Metering load	0 to 3 kN/m
Fluid delivery	Tank capacity	80 L
	Pump flow rate	0.16–0.5 L/s

The position of the metering rod is measured with two displacement transducers located at both ends. The position is given by the mean value of the two measurements, and is considered as correct if the difference is less than 10 μm. It corresponds to an angle of 2×10^{-3} deg between the revolution axes of the rod and the transfer roll. A reference position is initially obtained when both rolls are in contact and no load is applied. This position is approximately defined by the naked eye, with an uncertainty of ±20 μm. Then all measurements are fitted with the same bias, but repeatability gives a relative uncertainty of only ±3 μm. This position is controlled by modifying the load applied on the metering rod.

A piezotransducer (diameter 2.5 mm) is installed at the surface of the metering rod. In order to minimize intrusion effects, the membrane of the transducer was polished to fit the surface of the rod. The surface roughness, measured with a spindle micrometer, is less than 3 μm. The range of measurement is from -50 kPa to 700 kPa (relative to the atmospheric pressure), and the pressure transducer response time is 250 kHz.

The pressure data-acquisition procedure is as follows: a full single profile is acquired in the metering nip area at every rod revolution. This pressure profile is measured on a length of 20 mm, as shown in Figure 4. It contains 80 points, each of which is separated from the next one by 0.25 mm. Ten profiles are acquired successively. An average profile is obtained by computing the mean value at each point. The maximum uncertainty on this profile is 2% full scale, within a 95% confidence limit. By resetting all the parameters, the position of the rod, and the velocities of the rolls, pressure measurements are reproducible in a range of 3% full scale.

All the results reported in this work are obtained with Newtonian aqueous solutions of Polyethylene Glycol (PEG 35000 from Hermann Ter Hell & Co. GMBH). This model fluid was selected for its stable rheological properties, and ease to work with. The range of viscosity considered is from 20 mPa·s to 200 mPa·s, which is typical of the shear viscosity of a coating color in a MSP (200 to 400 mPa·s on a Brookfield viscometer with spindle 4 at 100 rpm) (Brown, 1996; Teirfolk and Vaito, 1996).

In order to describe the surface aspect of the coated layer on the transfer roll, a video imaging technique is used. The

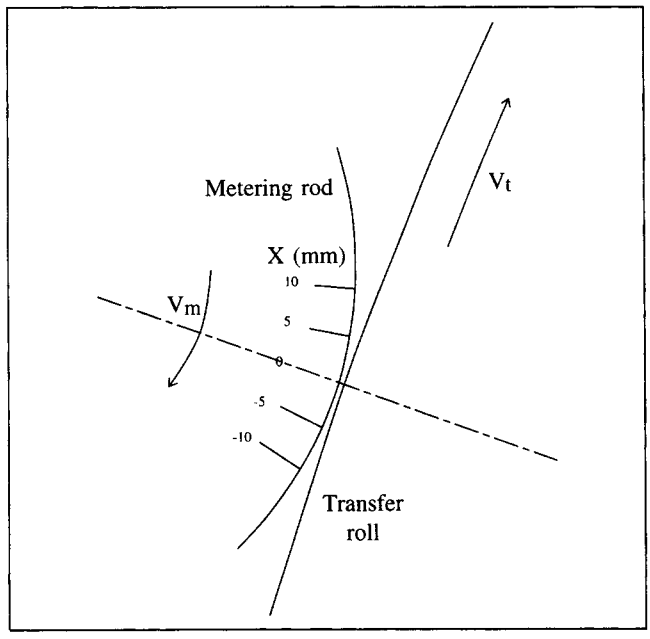

Figure 4. Reference diagram for pressure measurements.

surface of the layer at the exit of the nip is illuminated with a 250-W tungsten light, which makes the ribs appear in perspective, with bright and shaded areas. It is then possible to measure their width (or wavelength) and evaluate their amplitude. These two parameters are then used to quantify the degree of uniformity and assess the influence of the operating parameters.

The tungsten light and camera are set in an antisymmetric position with two different incidence angles, as represented on Figure 5, the first one (Figure 5a) to visualize a band of reflection, the second one (Figure 5b) to sharpen the edges of the illuminated parts of the ribs. This helps distinguish one rib from the next. Figure 6 describes what the camera can see. By capturing a 40-mm-long strip of this band of reflection, the width of a rib can be measured with fairly good accuracy. The measurement of the height of the illuminated part gives an indication of the amplitude of the ribs. Obtaining a relation between this height and the real amplitude is beyond our present capabilities. It would require a very good knowledge of light absorbency and diffusion in our fluid, and also an extremely accurate positioning of the camera and light projector.

When the coat layer is free of defects, a bright linear band appears on the full width of the roll. On the other hand, if the surface is ribbed, bright and shaded areas can be observed. As the height of the ribs increases, the band becomes larger, and shaded areas overlap each other. Images of the camera are recorded on a video and further processed with an image analysis system.

Figures 7a and 7b show two examples of ribbing patterns corresponding to the extreme cases we observed (smallest and largest nonuniformities, respectively). Due to the angle of incidence of the camera, the focus cannot be accurately set on the whole picture. It has been systematically optimized on the righthand side. The number of ribs is counted in this area, allowing the determination of the rib width. On the lefthand

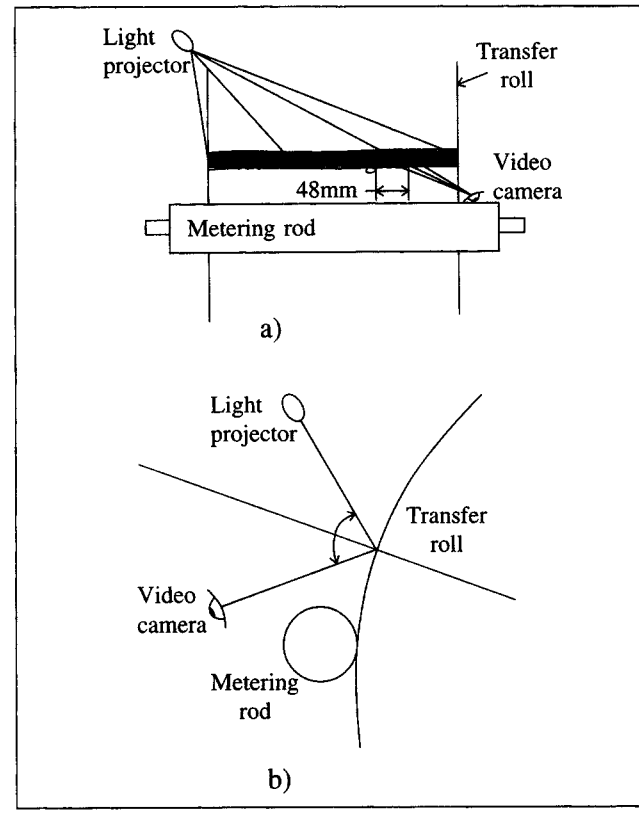

Figure 5. Visualization setup: (a) front view; (b) side view.

side, not only is the image fuzzy, but the shaded visible areas are also restricted due to the angle of perspective. Then, the reflection band becomes almost uniform, showing more diffuse small peaks. Such an area is well suited for measuring the height as defined in Figure 6.

Twenty-seven rib patterns were investigated in this work, corresponding to three different viscosities and nine combinations of transfer-roll and metering-rod velocities. The operating conditions, the width, and the height of the ribs measured are reported in Table 2.

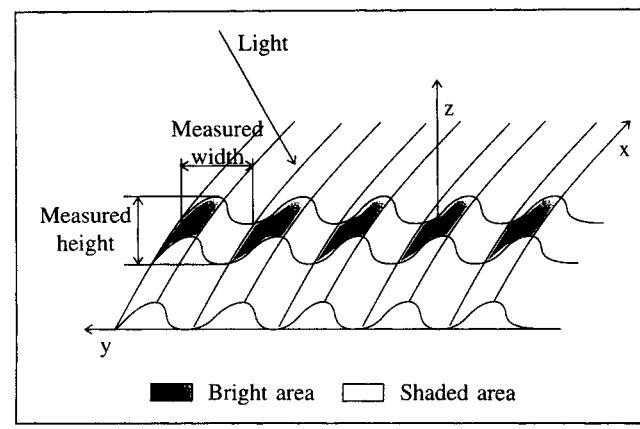

Figure 6. Visualization of the rib pattern.

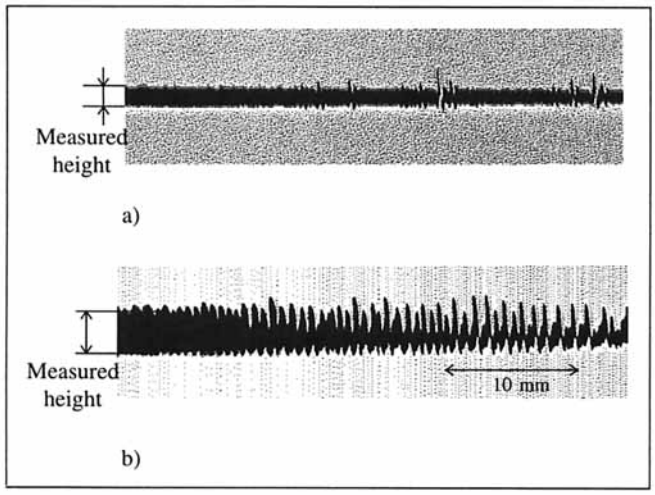

Figure 7. Minimum and maximum perturbation.

(a) V_t = 500 m/min; V_m = 60 m/min; μ = 125 mPa·s; (b) V_t = 1,000 m/min; V_m = 15 m/min; μ = 28 mPa·s.

Analysis of the Ribs

All the patterns obtained are systematically unstable to ribbing, as expected. Indeed, the critical capillary number, which would be predicted using Eq. 3 or alternatively the work of Coyle et al. (1990b), is about a hundred times lower than our experimental capillary number. The pattern obtained is also time-dependent in some cases (as far as we can identify it). The most obvious transient conditions occurred in the case of the larger width. One can see discrete cross-web nonuniform disturbances in Figure 7a. These perturbations are steady, and they appear in the case of the most stable to ribbing conditions. They are totally masked with significant unstable to ribbing conditions (Figure 7b).

From a qualitative standpoint, the operating parameters influence the ribs in the following way:

- An increase in the transfer roll velocity increases the height of the ribs, but does not significantly modify their width.
- The rib height and width can be reduced by lifting the metering-rod velocity.
- Modifying the gap thickness by changing the position of the metering rod, all other parameters being constant, does not produce any significant effect in the range considered ($H < 100$ μm).

Table 2. Rib Width and Height Measurements from Video Recordings

V_t (m/min)	500			750			1,000		
V_m (m/min)	15	30	60	15	30	60	15	30	60
μ = 28 mPa·s									
Width (mm)	0.63	0.49	0.45	0.67	0.52	0.46	0.71	0.52	0.49
Height (mm)	2.91	2.57	2.40	3.08	2.91	2.57	3.60	3.08	2.91
μ = 68 mPa·s									
Width (mm)	0.49	0.45	0.41	0.52	0.45	0.42	0.54	0.45	0.44
Height (mm)	2.05	1.95	1.95	3.08	2.31	2.20	3.25	2.73	2.40
μ = 125 mPa·s									
Width (mm)	0.44	0.42	0.41	0.44	0.43	0.43	0.45	0.43	0.43
Height (mm)	1.54	1.40	1.40	1.70	1.54	1.54	2.40	2.22	2.14

- Viscosity is a stabilizing factor in terms of width and height.

These observations globally give similar trends as those reported in the literature. The major influencing factors are, however, the metering-rod velocity and the fluid viscosity.

The data shown in Table 2 were processed to build a stability diagram (Figure 8a), following Coyle (1984). The results confirm that increasing the capillary number and/or the velocity ratio tends to reduce the flow disturbances (expressed as rib widths). However, no correlation was found when considering the measured heights. Ribbing patterns given in Figures 8b and 8c correspond to the same capillary number and velocity ratio. They appear very different. We found that the only reliable parameter that could explain this difference is the Reynolds number, defined as follows:

$$Re_m = \frac{\rho V_m H_r}{\mu}, \tag{4}$$

where H_r is a characteristic length (assigned arbitrarily the value of 100 μm). This number includes the critical parameters that were shown to influence the ribbing pattern the most, that is, the metering velocity and the viscosity.

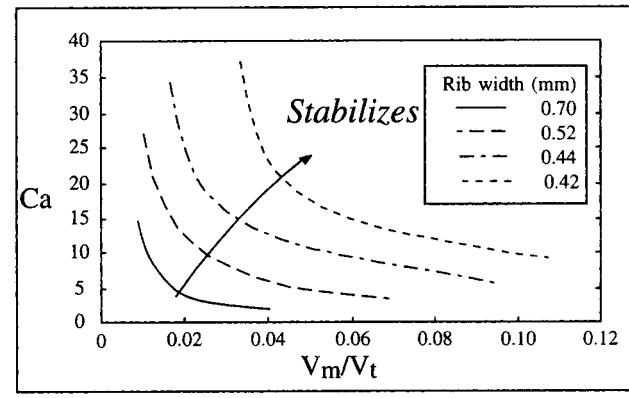

Figure 8a. Generalized stability (capillary number analysis).

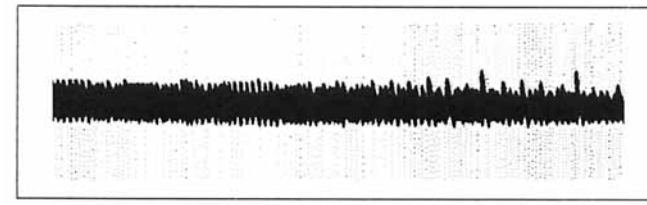

Figure 8b. Rib pattern: Ca = 8.5; V_mV_t = 0.03; Re_m = 0.38.

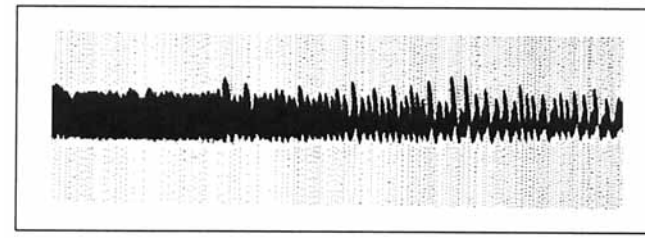

Figure 8c. Rib pattern: Ca = 8.5; V_mV_t = 0.03; Re_m = 1.87.

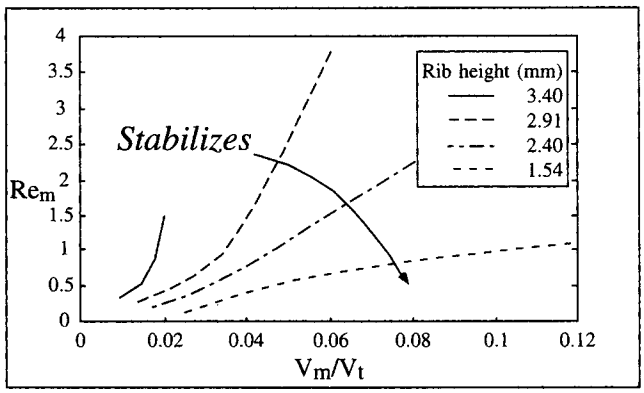

Figure 9a. Generalized stability (Reynolds number analysis).

Figure 9b. Rib pattern: $Ca = 35.3$; $V_m/V_t = 0.06$; $Re_m = 0.80$.

Figure 9c. Rib pattern: $Ca = 9.6$; $V_m/V_t = 0.06$; $Re_m = 0.80$.

Accordingly, we have reported in Figure 9a the measured ribs heights as a function of the velocity ratio and the Reynolds number. This particular stability diagram allows us to put the results in perspective; it can be observed that reducing the Reynolds number and/or increasing the velocity ratio tends to stabilize the flow pattern (decreasing the rib heights). Figures 9b and 9c illustrate the rib patterns at the same Reynolds number value and different values of the capillary number.

It should be noted here that the metering rod was kept in a fixed position. In other words, we did not consider any possible effect of the variation of the gap thickness. This gap thickness certainly varies with the transfer-roll velocity or when a fluid with a different viscosity is used. But, since variations of the metering-rod position did not show any significant effect on the rib width and height, we concluded that, in the configuration and operating range considered in the present work, the effects of the elastic deformation of the transfer-roll cover on the ribbing pattern were negligible.

Pressure-Profile Results

Knowledge of the nip pressure profile is very valuable in describing the nip flow hydrodynamic. It is also useful in practice since it allows us to assess how the load applied to the rod is evolving when an operating parameter is changed. Pressure-profile measurements are first carried out to examine the effects of the different operating parameters on the hydrodynamic patterns. Figures 10a to 10d show the evolution of the pressure when the transfer-roll and metering-rod velocities V_t and V_m, the metering rod position H, and the viscosity of the fluid μ are varied. The results can be summarized as follows:

- The maximum pressure increases almost linearly when V_t increases, H decreases, and/or μ increases.
- The bandwidth (length of the nip with positive pressure), increases when V_t increases, H decreases, and/or μ increases.
- A minimum subatmospheric pressure appears in the second half of the nip when V_t increases, V_m decreases, and/or μ decreases.
- This minimum pressure is followed by a local pressure peak before the exit of the nip.

In the major part of the nip, where the pressure is positive, the transfer-roll velocity and the viscosity yield comparable effects, that is, a normal load at the rod develops while increasing this velocity (or using a more viscous fluid). This load increases the compression of the transfer-roll cover, which in turn makes the gap become thicker and also slightly longer in the machine direction. Decreasing the gap thickness by applying more load on the metering rod yields similar results. Finally, due to the low value of the velocity ratio V_m/V_t, it is not surprising that V_m has so little effect on the overall shape of the pressure profile.

In the small region where the pressure is subatmospheric, the trends are quite different from those just cited, but very similar to the ones obtained from the stability analysis: increasing the metering-rod velocity or using a more viscous fluid leads to a reduced minimum pressure and also tends to stabilize the ribbing pattern. Conversely, an increase in the transfer-roll velocity augments the subatmospheric pressure and also tends to destabilize the flow. The position of the metering rod, H, is not a significant factor in both cases. These observations confirm, as was found earlier by Pitts and Greiller (1961), that a positive pressure gradient at the exit of the nip tends to destabilize the flow and generates ribbing.

The flow pattern in the nip can be described as illustrated in Figure 11: both maximum and minimum pressures delimit the area where there is no recirculation. Indeed, at these extremums, the pressure gradient dP/dx is locally equal to zero, and therefore the velocity profile is linear. The contact line between the meniscus and the metering rod is located where the pressure is constant (Figure 10), between 4 and 6 mm from the center of the nip.

We know, from the literature (Coyle et al., 1990b), that a perturbed two-dimensional flow under the meniscus may become three dimensional and eventually time dependent. The Reynolds number Re_m characterizes the activity of these three-dimensional recirculations. The use of a more viscous fluid lowers Re_m, and then offsets inertia effects. The consequence of increasing the metering-rod velocity is to move the contact line backwards through the nip, restricting the region where the recirculations occur. It also reduces the minimum nip pressure, following some mechanism not yet clearly iden-

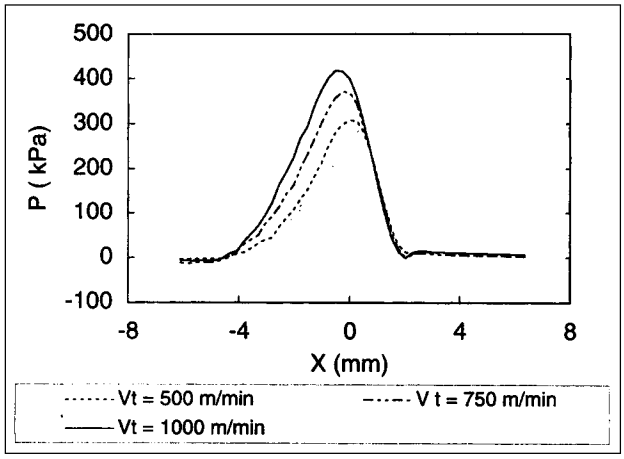

Figure 10a. Effect of V_t on the pressure ($V_m = 30$ m/min; $H = 0$ μm; $\mu = 68$ mPa·s).

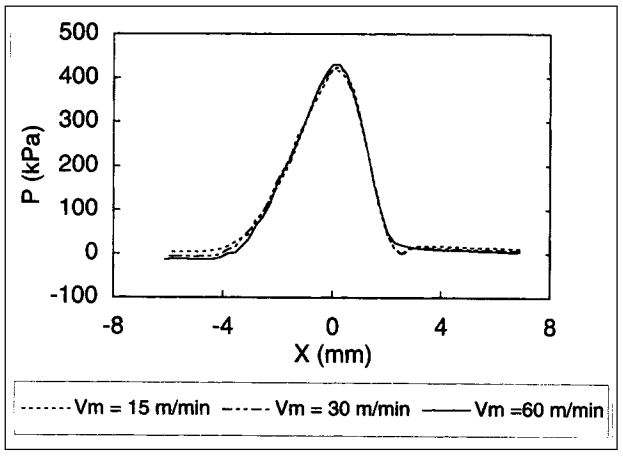

Figure 10b. Effect of V_m on the pressure ($V_t = 1{,}000$ m/min; $H = 0$ μm; $\mu = 68$ mPa·s).

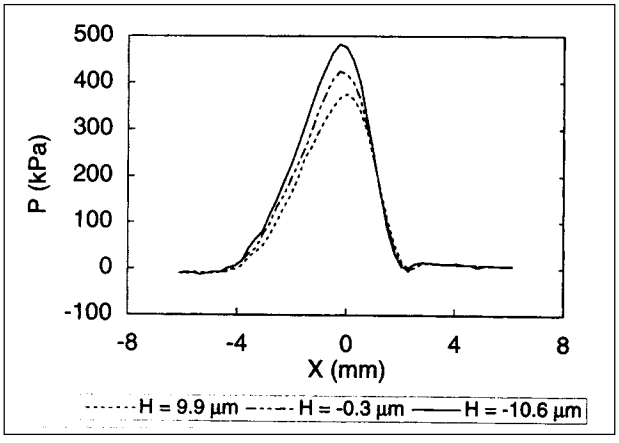

Figure 10c. Effect of H on the pressure ($V_t = 1{,}000$ m/min; $V_m = 30$ m/min; $\mu = 68$ mPa·s).

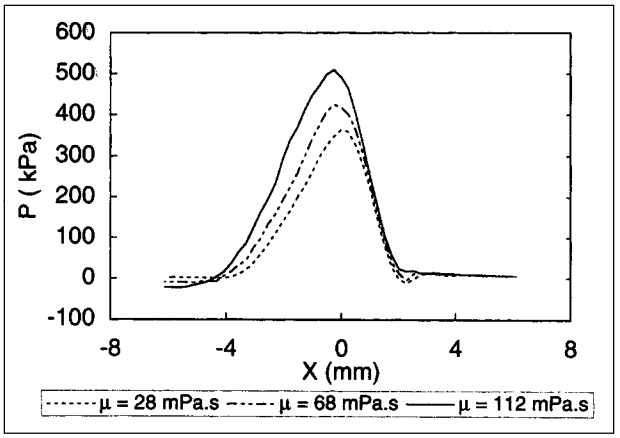

Figure 10d. Effect of μ on the pressure ($V_t = 1{,}000$ m/min; $V_m = 30$ m/min; $H = 0$ μm).

tified, but possibly linked to these three-dimensional flow recirculations.

In coating studies, capillary effects are generally taken into account to describe the ribbing pattern. In this work, the variation of the capillary number, obtained by modifying the roll velocities while maintaining their ratio constant, showed very little effect on the minimum pressure. This can probably be explained by the fact that the roll-velocity ratio is very small, and the meniscus remains relatively far from the nip center. No minimum pressure peak means that there is no divergence of the streamlines while escaping from the nip.

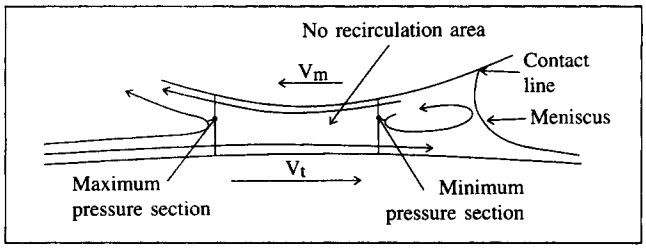

Figure 11. Flow pattern.

Geometrical changes in the nip, due to the deformation of the cover on the transfer roll, do not play any significant role in the operating range, as the position of the metering rod showed no influence on the minimum pressure. In fact, it looks like applying more load on the metering rod does not modify the geometry of the gap, at least in the range of the nip gap investigated.

Influence of operating conditions

In order to assess the effect of the operating conditions on the flow, the relation between the maximum pressure and the operating parameters V_t, V_m, and H was examined for different fluid viscosities. Results are reported in Figures 12 to 15.

Figures 12a and 12b show the effects of the position of the metering rod on the maximum pressure for different values of V_t and μ. These graphs reveal the existence of two different regions where the pressure varies linearly. The critical value H^* bounding the two regions depends mainly on V_t and slightly on μ. It can be defined by the following relation:

$$H^* = \frac{2(V_t - 750)}{25}. \tag{5}$$

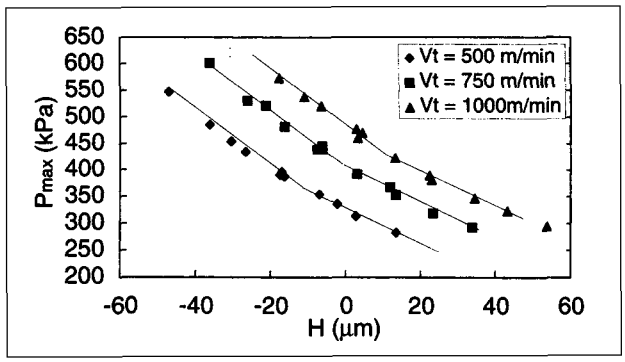

Figure 12a. Effect of the metering-rod position on P_{max}: $V_m = 30$ m/min; $\mu = 95$ mPa·s.

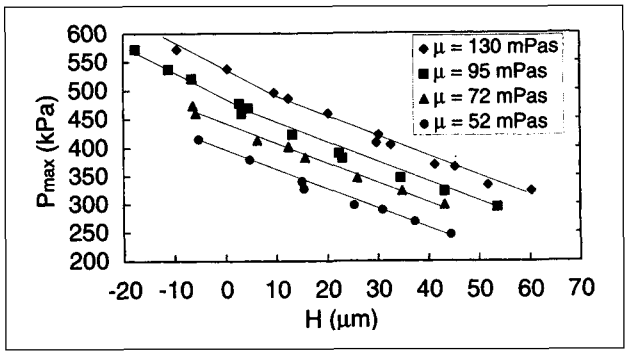

Figure 12b. Effect of the metering-rod position on P_{max}: $V_t = 1{,}000$ m/min; $V_m = 30$ m/min.

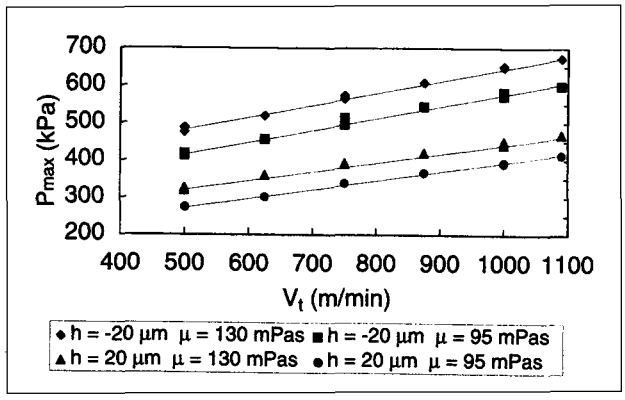

Figure 12c. Effect of the transfer roll velocity on P_{max}: $V_m = 30$ m/min.

We believe that H^* could be related to the positive and negative gaps reported in the literature (Carvalho and Scriven, 1993); in other words, to a gap-geometry transition.

From the last plots, the following slopes can be deduced:

$$\frac{\Delta P_{max}}{\Delta H} = -3.2 \text{ kPa}/\mu\text{m} \qquad H > H^*$$

$$= -5.0 \text{ kPa}/\mu\text{m} \qquad H < H^*. \qquad (6)$$

Figure 12c shows the effect of V_t on the maximum pressure for two viscosities in the two gap regions evidenced in Figure 12a. Again, the maximum pressure increases almost linearly over the range considered. The slopes are

$$\frac{\Delta P_{max}}{\Delta V_t} = 15.0 \text{ kPa}\cdot\text{s/m} \qquad H > H^*$$

$$= 20.4 \text{ kPa}\cdot\text{s/m} \qquad H < H^*. \qquad (7)$$

In Figure 13, we show the variation of the maximum pressure vs. the viscosity for three transfer-roll velocities and three gap thicknesses. Looking at Figure 13a, where the lines plotted are not parallel, it seems that the ratio $\Delta P_{max}/\Delta\mu$ depends on V_t. In reality, this graph corresponds to the transition region where H is close to H^*. Figures 13b and 13c correspond, respectively, to the thin- and wide-gap regions, and the pressure slopes are constant in each case. Table 3 summarizes the ratios obtained with the four viscosities and the different positions of H relative to H^*.

From the plots at $H = 20$ μm (Figure 13b) and $H = -20$ μm (Figure 13c), we obtain the following ratios:

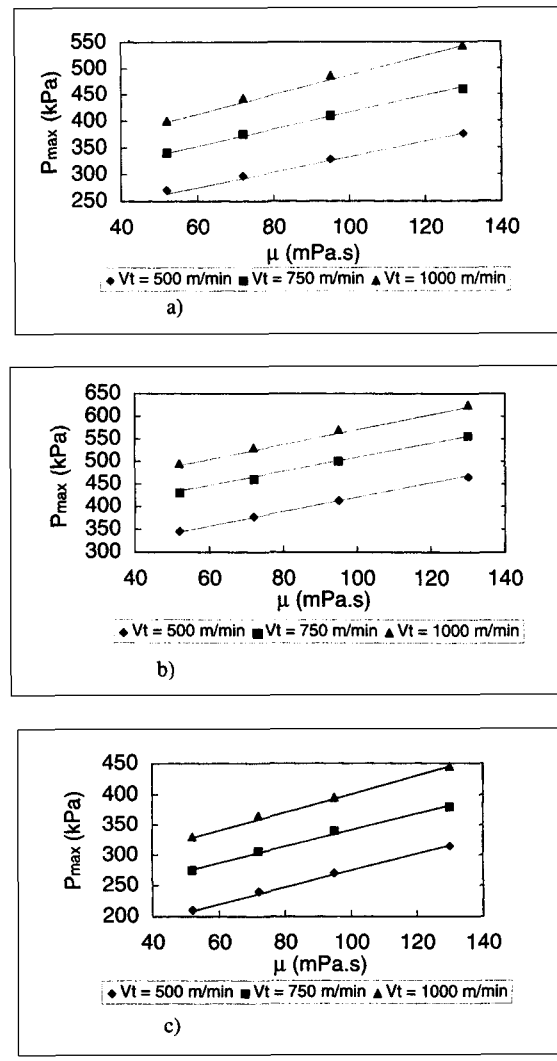

Figure 13. Influence of the viscosity on P_{max}: (a) $H = 0$ μm; $V_m = 30$ m/min; (b) $H = -20$ μm; $V_m = 30$ m/min; (c) $H = 20$ μm; $V_m = 30$ m/min.

Table 3. Apparent Effects of H on $\Delta P/\Delta V_t$

$\Delta P_{max}/\Delta V_t$ (kPa·s/m)	μ (mPa·s)	
15.6	52	$H > H^*$
17.4	72	$H \approx H^*$
18.6	95	$H \leq H^*$
19.2	130	$H < H^*$

$$\frac{\Delta P_{max}}{\Delta \mu} = 1.4\times10^6\ s^{-1} \qquad H > H^*$$

$$= 1.8\times10^6\ s^{-1} \qquad H < H^*. \tag{8}$$

Finally, Figure 14 shows the influence of V_m on P_{max} for four different viscosities. Here again, there is a linear increase in P_{max}, but this time with some clear dependence on μ:

$$\frac{\Delta P_{max}}{\Delta V_m} = 0.512\mu - 7.02 \quad \text{kPa·s/m}. \tag{9}$$

One can notice that this ratio is at least as important as $\Delta P_{max}/\Delta V_t$ for the small viscosities, and can be as much as three times bigger for the large ones. The effect of V_m is very small, as this velocity does not vary much as compared to V_t. So V_m has almost no influence on the geometry of the gap. Consequently, the relation between μ and $\Delta P_{max}/\Delta V_m$ is an indication that V_m influences in some manner the flow pattern. This complies with our previous stability analysis using the Reynolds number (Figure 9).

Using the whole set of data just presented, it is possible to derive a general equation giving the maximum pressure for any set of parameter values:

$$P_{max} = P_0 + \frac{\Delta P_{max}}{\Delta V_t}(V_t - V_{t0}) + \frac{\Delta P_{max}}{\Delta \mu}(\mu - \mu_0) + \frac{\Delta P_{max}}{\Delta H}(H - H_0), \tag{10}$$

where the subscript "0" corresponds to a reference value obtained experimentally. This equation gives a good fit of the experimental results. An attempt was made to use the equations of lubrication, but this approach failed to represent our data. Here again, we suspect some strong effects of inertia. This point will be addressed in future work.

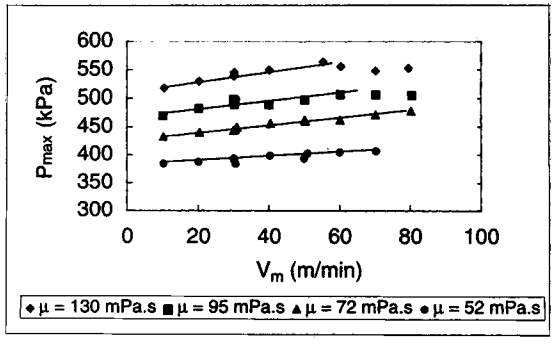

Figure 14. Metering-rod velocity effects on P_{max}: V_t = 1,000 m/min; $H = 0$ μm.

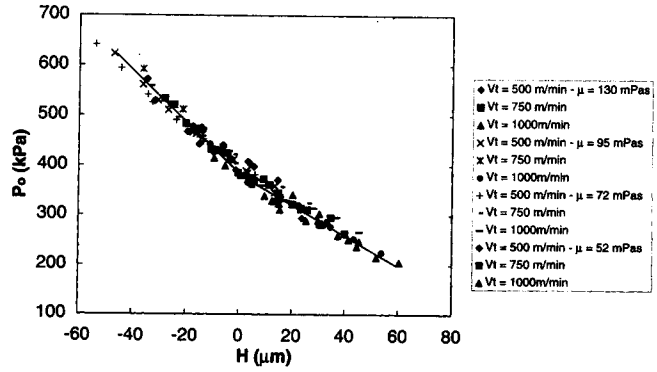

Figure 15. Pressure master curve (reference data: V_{t0} = 750 m/min; V_{m0} = 30 m/min; μ_0 = 90 mPa·s).

One master curve, representing for example, P_{max} as a function of H, could be deduced from Eq. 10. It represents a piece of information useful in design practice. As an illustration, Figure 15 represents such a master curve for $V_m = 30$ m/min. The discrepancy error is evaluated at 8%, 3% of which corresponds to the measurement error. The 5% left is related to the error on slopes and nonlinear effects. Moreover, as mentioned earlier, the absolute value of H is unknown at ± 20 μm. This would simply result in shifting the curve less than 20 μm on the right or on the left.

Comparison with results of Carvalho and Scriven

We now compare our pressure measurements against the dimensionless approach of Carvalho and Scriven (1993). We recall that their model considers a viscous fluid flow, an elastic transfer roll cover deformation, and uses the lubrication assumptions. Two dimensionless groups are proposed for the pressure, depending on the nip configuration, namely, $(PR/\mu V)$, for the positive gap, and (PL/ER), for the negative gap, where L is the transfer-roll cover thickness.

The first dimensionless group could not be used in our case. Indeed, if we consider any of our results at a given metering-rod position and two different fluid viscosities (for a given value of the elastic number), such dimensional representation gives two different pressure profiles. This can be verified, for example, with the maximum pressure measurements plotted on Figure 13c: at $V_t = 500$ m/min at $\mu = 120$ mPa·s or at $V_t = 1{,}000$ m/min and $\mu = 60$ mPa·s, the elastic number is identical for both points ($Ne = 6\cdot10^{-6}$), but the corresponding maximum pressure measurements differ by 12%. Which profile should then be used in the dimensionless representation? In fact, we confirm here that the lubrication theory does not fit with our application. A dimensionless form should probably include an inertial contribution.

The second dimensionless group is then used for comparison purposes. We show in Figure 16 the dimensionless pressure profile vs. the nip length. It should be noted that the model of Carvalho and Scriven was adjusted to fit our nip geometry. It can be seen that the computed maximum nip pressure is somewhat lower but in the same range as our experimental measurement.

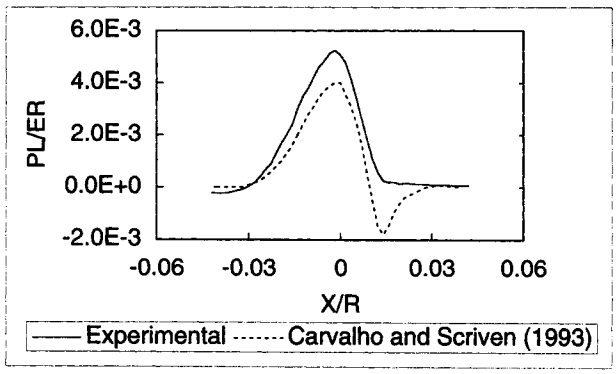

Figure 16. Experimental pressure profile: $Ne = 7 \times 10^{-7}$; $H/R < 10^{-4}$; numerical data (Carvalho and Scriven, 1993): $Ne = 10^{-6}$; $H/R = -2 \times 10^{-4}$.

Conclusion

A high-speed experimental apparatus was developed to examine the flow in the metering unit of a MSP. Hydrodynamic investigations gave quantitative information concerning the stability of the flow.

The pressure profile measurements revealed some interesting features. First of all, considering the maximum pressure only, a transition was identified by a change of slope for the graphs of maximum pressure with respect to the different operating parameters. This transition is defined by the value H^* of the position of the metering rod where this change of slope occurs. H^* depends on the transfer roll velocity, but not on the viscosity, when the metering rod velocity is kept constant. Two elements might explain this behavior: the deformation of the elastomer due to the normal load developed in the flow, and the location of the back flow under the meniscus.

On the other hand, the effects of V_m for a constant value of H were investigated. It was shown that varying V_m has an impact on the stability of the layer as well as on the value of the minimum pressure.

Video analysis was used to quantify the instabilities. Stability diagrams confirmed that in the operational range of a metering-size press, where the velocity ratio V_m/V_t is very small (less than 0.1), the gap thickness is very small ($H/R < 10^{-4}$), and inertia effects become significant and potentially predominant in the stability analysis.

Other parameters that have not been taken into account, but may interfere in the flow-stability analysis, include the stiffness of the elastomer and the size of the metering rod. A harder elastomer would certainly increase the value of H^*, yielding stronger instabilities. A smaller rod would probably reduce the maximum and minimum pressure values and then stabilize the layer, provided slippage effects on the rod were not overwhelming. These factors will have to be taken under close consideration.

Acknowledgments

The financial contribution of Paprican and NSERC and the technical assistance of McMillan-Bloedel are grateful acknowledged.

Notation

H_r = length scale of the gap thickness at the exit of the nip
P = pressure in the nip
P_{max} = maximum pressure in the nip
P_0 = maximum reference pressure
V_{t0} = reference velocity of the transfer roll
ρ = density
μ_0 = Newtonian reference viscosity
σ = surface tension

Literature Cited

Aidun, C. K., "Principles of Hydrodynamic Instability: Application in Coating Systems: 1. Background," *TAPPI J.*, **74**(3), 213 (1991a).
Aidun, C. K., "Principles of Hydrodynamic Instability: Application in Coating Systems: 2. Examples of Flow Instability," *TAPPI J.*, **74**(4), 213 (1991b).
Benkreira, H., M. F. Edwards, and W. L. Wilkinson, "Ribbing Instability in the Roll Coating of Newtonian Fluids," *Plastic Rubber Proc. Appl.*, **2**, 137 (1982).
Brown, J. T., "Metered Size Press Pilot Study," *TAPPI Coating Conf. Proc.*, Nashville, TN, p. 13 (1996).
Carvalho, M. S., and L. E. Scriven, "Effect of Deformable Roll Cover on Roll Coating," *TAPPI Coating Conf. Proc.*, Minneapolis, p. 451 (1993).
Conlisk, A. T., and M. R. Foster, "The Steady Flow in a Short-Dwell Coater II—Web Pressure Distribution and Flow Under the Blade," *TAPPI Coating Conf. Proc.*, Montreal, p. 327 (1991).
Coyle, D. J., "The Fluid Mechanics of Roll Coating: Steady Flows, Stability and Rheology," PhD Thesis, Univ. of Minnesota, Minneapolis (1984).
Coyle, D. J., "Forward Roll Coating with Deformable Rolls: A Simple One-Dimensional Elastohydrodynamic Model," *Chem. Eng. Sci.*, **43**, 2673 (1988).
Coyle, D. J., C. W. Macosko, and L. E. Scriven, "The Fluid Dynamics of Reverse Roll Coating," *AIChE J.*, **36**(2), 161 (1990a).
Coyle, D. J., C. W. Macosko, and L. E. Scriven, "Stability of Symmetric Film-Splitting Between Counter-rotating Cylinders," *J. Fluid Mech.*, **216**, 437 (1990b).
Eklund, W. R., H. A. LeBlanc, and D. G. Halley, "The Cylindrical Laboratory Coater—A New High Speed Blade Coater for the Laboratory," *TAPPI Coating Conf. Proc.*, New Orleans, p. 81 (1988).
Greener, J., T. Sullivan, B. Turner, and S. Middleman, "Ribbing Instability of a Two-roll Coater: Newtonian Fluids," *Chem. Eng. Comput.*, **5**, 73 (1980).
Kustermann, M. F., and W. A. Damrau, *TAPPI Coating Conf. Proc.*, San Diego, p. 197 (1994).
Mill, C. C., and G. R. South, "Formation of Ribs on Rotating Rollers," *J. Fluid Mech.*, **28**, 523 (1967).
Miura, H., and C. K. Aidun, "Pressure Fluctuations and Coat-Weight Nonuniformities in Blade Coating," *TAPPI Coating Conf. Proc.*, Orlando, p. 209 (1992).
Pearson, J. R. A., "The Instability of Uniform Viscous Flow under Rollers and Spreaders," *J. Fluid Mech.*, **7**, 481 (1960).
Pitts, E., and J. Greiller, "The Flow of Thin Liquid Films Between Rollers," *J. Fluid Mech.*, **11**, 33 (1961).
Salminen, P., R. Urscheler, J. Roper III, and D. Chase, "Optimizing the Coating Formulation to Reduce Misting in High-speed Film Coating," *TAPPI Coating Conf. Proc.*, Nashville, p. 51 (1996).
Teirfold, J. E., and L. Vaito, "An Empirial Study of Blade Coating at 2250 m/min," *TAPPI J.*, **79**(2), 206 (1996).

Manuscript received Oct. 7, 1996, and revision received July 11, 1997.